# Design of a passive add-on ring for imbalance suppression

Group A8: M. van der Helm (4481860), R. Meijer (4431804), S.J. van der Voort (4442296) and J. Montagne (4455576)

June 6, 2019

***Abstract*—This study describes the design of a passive add-on ring for imbalance suppression, applied to the rotating parts of a clinical centrifuge. The vibrations caused by this imbalance can be reduced by means of a passive add-on ring. The development of a numerical model that describes the dynamics of a general rotor-imbalance system allowed for an effective design process. The model has been verified by practical experiments, using a prototype add-on ring with dimensions as predicted by the model. Using this method, the aforementioned vibrations have been reduced by up to 75%, while the error margin increased by 150%.**

## I. Introduction

Imbalance in rotating devices can cause unwanted vibrations that influence both device life-expectancy as well as quality of the product. Industrial examples of devices that fit this description are washing machines and DVD-drives. In these devices, an Automatic Ball Balancer (ABB) is often used to prevent these issues [1]. In clinical practise, Platelet Rich Fibrin (PRF) extraction is deemed a promising method of accelerated soft tissue healing and bone reconstruction [2][3]. This method is used in applications such as oral surgery and orthopedic, cosmetic and dermatological interventions. Blood is extracted from the patient and stored in test tubes. Usually, 20-120 ml of blood is spread over 2-12 tubes, in which the blood clots rapidly when outside of the human body. Blood separation is achieved by spinning the tubes at 1400 RPM for 12 minutes. It is essential that the tubes are well-balanced in order ensure proper separation of white blood cells and platelets from the residue [4]. This balancing procedure can be tedious and time-consuming. The goal is therefore to allow for larger imbalances, so that the physician saves valuable time, without increasing the intensity of system vibrations. This can be achieved by design and implementation of an add-on ring that follows the ABB principle, with parameters as predicted by a numerical model. This leads to the research question: *How can one, using a dynamic model and practical experiments, predict and reduce vibrations caused by a rotating constant imbalance?*

## II. Design of the add-on ring

The design of the add-on ring is based on the working principle of an ABB, which can be described by means of a rotor model. The model used in this study assumes a stiff motor axle and weak connection between axle and rotor, contrary to the Jeffcott model, which assumes a stiff connection and weak axle [5]. As shown in Figure 1, point *A* represents the center of rotation, point *B* the geometrical center and point *C* the combined Center of Gravity (CoG) position of all imbalances acting on the rotor.

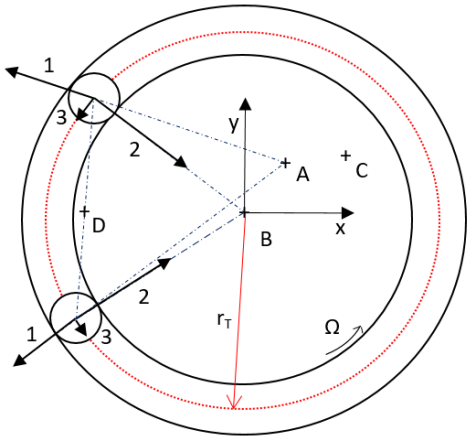


Figure 1: *Dynamics of an imbalanced rotor with ABB*

As a result of the offset of point *C*, center of rotation *A* will not coincide with geometrical center *B*, causing vibrations. The magnitude of this vibration can be approached by using *C* as point of engagement for the centripetal force ($F_{c,im}$) [6], in accordance with equation 1.

$$F_{c,im} = \frac{m_{im} * v_{im}^2}{r_{BC}} \tag{1}$$

The force $F_{c,im}$ is dependent on the mass ($m_{im}$, in [kg]) and rotational speed ($v_{im}$, in [m/s]) of the imbalance, as well as the distance between *B* and *C* ($r_{BC}$, in [m]).

High rotational speeds cause this force to be dominant in the rotor-imbalance system, as opposed to the much smaller and constant gravitational force. Equation 1 holds true when using a rotating frame, fixed to the rotor. In order to detect the vibrations, a transformation to a non-rotating frame with fixed x- and y-axes is applied. This yields equations 2 and 3.

$$F_x = \cos(\theta + \phi) * \frac{m_{im} * v_{im}^2}{r_{BC}} \tag{2}$$

$$F_y = \sin(\theta + \phi) * \frac{m_{im} * v_{im}^2}{r_{BC}} \tag{3}$$

In these equations, $\phi$ is the angle between point *C* and the x-axis of the rotating frame, where $\theta$ describes the angle between the x-axes of the rotating- and fixed-frame. Both equations 2 and 3 now yield a sinusoidal vibration

force, with the amplitude determined by $F_{c,im}$ and period given by the RPM setting of the device.

In order for the system to be balanced, points *A* and *B* must coincide. This can be achieved by introducing the add-on ring. The ring features a track with radius $r_T$ and at least two identical balls that can freely move along the track, with combined mass $m_{balls}$. This, along with the angle between the balls and the x-axis of the rotating frame, determines the location of the combined CoG of the balls (*D*). The distance between *B* and *D* ($r_{BD}$) are variable because the balls can move freely.

Vectors *(1)* and *(2)* cause a resultant force vector *(3)* to act upon each ball, which 'pushes' the balls around the track. This causes movement of point D until steady-state is reached. Force vector (1) is an apparent centrifugal 'force', experienced by the balls and caused by inertia effects [5]. Vector *(2)* describes the normal force exerted by the track on the balls, perpendicular to the point of contact.

Suppose a rotating system with velocity $v_i$, where $m_{balls} = m_{im} \neq 0$. When steady-state is reached, the balls meet their equilibrium points. With the balls not moving, $v_{im}$ equals $v_{balls}$. The system must satisfy equation 4 for it to be balanced, in accordance with equation 1.

$$\frac{m_{im} * v_{im}^2}{r_{BC}} = \frac{m_{balls} * v_{balls}^2}{r_{BD}} \tag{4}$$

The terms $v_{im}$ and $v_{balls}$ cancel each other. Remember that the distance $r_{BD}$ can be variable. Rewriting equation 4 to equation 5 yields that $m_{balls} \geq m_{im}$, by virtue of $r_{BD}$ being variable, in order for the system to be completely balanced when $r_{BC} \leq r_{BD}$:

$$m_{balls} = \frac{m_{im} * r_{BC}}{r_{BD}} \tag{5}$$

## III. Simulation and Experiments

Simulations are combined with experimental tests in order to reduce the amount of add-on ring design iterations. In the simulation, specifications of a PRF-centrifuge are used to form the basis of the dynamic rotor model. In the experiments, the centrifuge is used to verify the performance of a prototype ring.

### A. Simulation

The rotor model is simulated with varying test tube imbalance, in order to better understand the dynamics and behaviour of the vibrations. In Table 1, a brief overview of impactful parameters has been given.

Table 1: *Parameters used during simulation and testing*

| Parameter | Symbol | Value range | Unit |
|---|---|---|---|
| Track radius | $r_T$ | 110 | mm |
| Mass per ball | $m_b$ | 0.25 - 1.5 | g |
| Mass of imbalance | $m_i$ | 0 - 8 | g |

Figure 2 results from a simulated ring with a track radius $r_T$, 2 balls of 7 g each, and suggests that this configuration is able to counter an imbalance of 5 g completely, corresponding with equation 5. Vibrations become non-allowable when they exceed 0.6 N, after which the machine starts shaking violently.

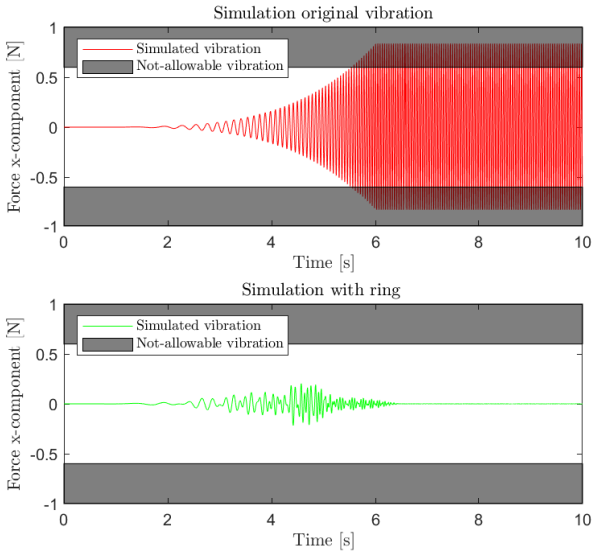


Figure 2: *Model predictions of add-on ring performance*

### B. Test setup

The centrifuge was centered as much as possible while being mounted on a three Degrees of Freedom (3-DoF) force sensor. The sensor measured linear forces in x-, y- and z-direction. Sensor data was logged using the included Optoforce sensor software and processed using Matlab. The sensor and centrifuge were connected using two grade 7075-T6 Aluminium coupling pieces. Furthermore, the setup was secured to a rigid wooden base and fastened to a table using glue clamps, in order to suppress ambient vibration noise and system resonance. See Figure 3 for an overview of the test setup.

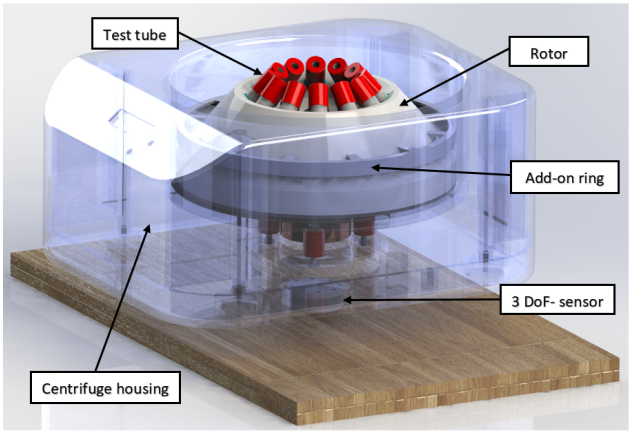


Figure 3: *Overview of the test setup*

The add-on ring was 3D-printed using Accura Xtreme ABS. Subsequently, the ring was fine-sanded and dust-cleared. A secure bond between the ring and rotor face was achieved by using strong double-sided tape.

### C. Experiments

Experiments were conducted in the following order: establishing baselines, analyzing vibrations, stiffening mounting points, testing add-on ring prototype. The RPM count of the centrifuge could be adjusted in the range of 300 to 4500 RPM. All experiments used the 1400 RPM setting unless specified otherwise, as this is the speed used in the PRF extraction method.

During baseline experiments, the rotor was spun without added imbalance. The baseline tests were executed in order to identify sensor and system noise.

According to equation 1, only two system variables can be altered. The first vibration analysis experiment varied the mass of the imbalance by filling the test tubes to different amounts. The effect of rotational velocity was analysed at constant imbalance and varying centrifuge RPM settings. The radius of the imbalance is dependent of the mass of the imbalance and therefore cannot directly be varied.

The mounting points of the driving motor and axle were stiffened after it became apparent that these were not rigid enough for stiff axle assumptions, significantly affecting experiment results. With stiffened mounting points, the experiments with varying imbalance mass were repeated. The last series of experiments continued with the stiffened mounting points and included the add-on ring. Tests with varying ball mass were conducted in order to analyze add-on ring behaviour.

## IV. Results

### A. Imbalance Analysis

Figure 4 shows the vibration forces in x-direction during a 20 second steady-state window of an experiment with 1 g test tube imbalance, at 1400 RPM. This window excludes the transient system behaviour of both the startup and slowdown phase. The steady-state window lasts 12 minutes, in which the blood clots and separates, completing the PRF separation process. Hence, our interest lies in reducing vibrations in this window. The figure shows the noisy signal $F_x$, which will now be filtered to the estimated signal.

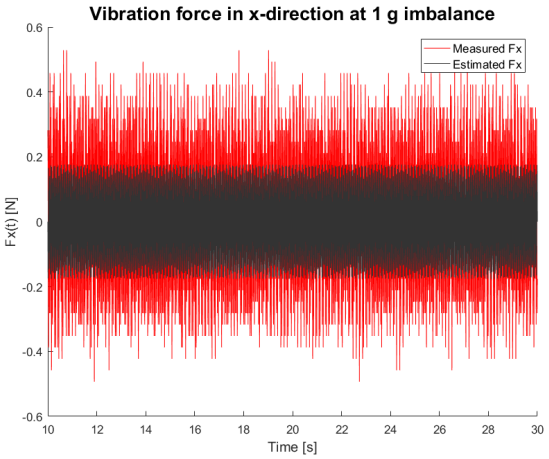


Figure 4: *Vibration forces in time domain*

The estimation process follows the Fast Fourier Transform algorithm. The time-domain sensor signal is converted to frequency domain, as can be seen in Figure 5. The absolute magnitude of $F_x$ is plotted against the frequency at which these forces occur. In the figure, a peak at 23 Hz can be distinguished, which converts to approximately 1400 RPM. This coincides with the rotational speed of the test tube imbalance. The baseline tests revealed that noise occurred at frequencies between 5 and 10 Hz [7]. This way, the magnitude of the vibration caused by this imbalance can be deduced and the force values caused by sensor noise and default system imbalance can be filtered out.

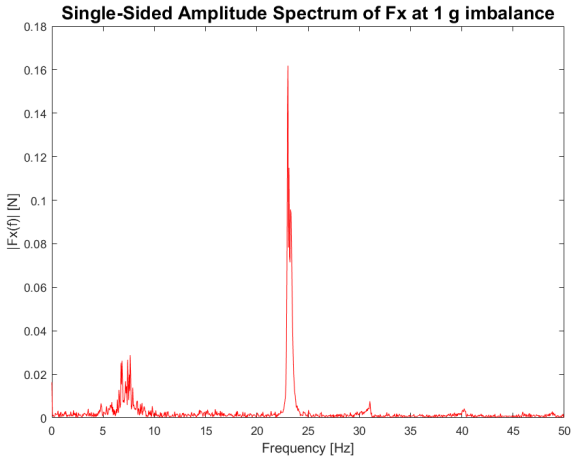


Figure 5: *Vibration forces in frequency domain*

### B. Simulation-Experiment comparison

The predicted vibrations were compared to the experimental data in order to validate the numerical model, as shown in Figure 6. These show large discrepancies, mostly as a result of sensor noise.

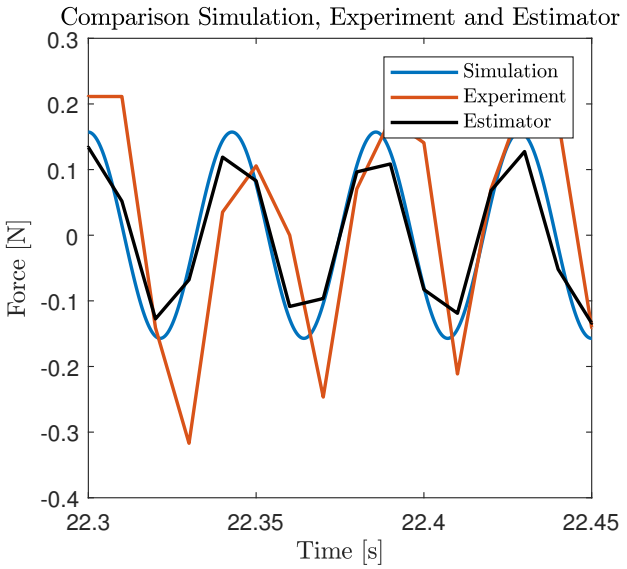


Figure 6: *Comparing predicted, measured and corrected vibrations*

After estimating the actual vibrations by filtering out the noise, a discrepancy can be seen in the order of 0.05 N, which is well within a 10% error margin of most system vibrations. The added robustness of the add-on ring causes the model to be a sufficient predictor for system vibrations.

### C. *Stiffening and Ring tests*

The motor and driving shaft were initially mounted on flexible rubber legs. At low amounts of imbalance - less than 1 g - this appears to effectively combat vibration forces. At larger imbalances however, the rubber legs further amplify the initial vibrations. After stiffening the motor mounting, vibration forces recorded by the sensor decreased. The mounting points were stiffened by adding 7075-T6 grade Aluminium mounting points that envelop the flexible rubber ones. The add-on ring was tested after the mounting was stiffened. The results are combined with those of the stiffened mounting (without add-on ring) and the original findings in Figure 7.

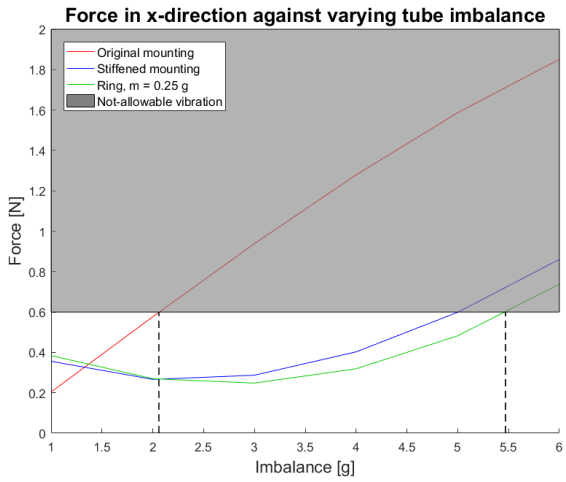


Figure 7: *Performance improvement steps*

The figure suggests that the biggest decrease follows after stiffening the mounting points. However, at larger imbalances the add-on ring still contributes to further balance the system. The bandwidth for operation under 0.6 N has increased from 2 to 5.5 g of imbalance. Vibration forces have been reduced from 1 to 0.25 N at 3 g imbalance. For imbalances less than 1.2 g, it might still be beneficial to choose the non-stiffened mounting.

## V. Discussion

Surprisingly, the largest decrease in vibration force was not caused by the add-on ring, but followed after stiffening the motor mounting points. The ring behaviour experiments were conducted using multiple ball diameters, as well as a varying number of balls. The latter did not provide enough data for this study to draw valuable conclusions. It is therefore recommended that future research focuses on this subject. While the model was able to accurately describe system vibrations, it could not predict add-on ring behaviour to a satisfying degree, leading ring performance to be less than expected beforehand. Possible discrepancies are the effects of: roll friction, fluid dampening, track section profile and test setup interference. Further recommendations would be to investigate the influence and origin of the previously mentioned model-experiment discrepancies and to expand the model with optimization algorithms. Extensive reports on mounting point stiffening, test results and further considerations can be found in the Supplemental Information [7].

## VI. Conclusion

The add-on ring has been designed, produced and tested. The numerical model was able to accurately predict vibrations, but had trouble predicting exact ring behaviour. Combining the predictive model with practical experiments provided insights in the working principle of the ABB and discrepancies between model and experiments. The largest decrease in vibration force occurred after changing the flexible mounting points to sturdier alternatives. For the PRF use case - with imbalance up to 5 g - it is recommended to use a stiffened motor mounting with add-on ring. The PRF-centrifuge allows for up to 2.5x as large of an imbalance in this configuration when compared to initial conditions. Therefore, it offers an increased margin of error for the operator. At the same time, vibration forces have remained within tolerable amounts. The device saw a force reduction of up to 75 percent, ensuring extended machine lifetime and maintaining quality of blood separation.

## References

[1] H. Lindell. *Automatic balancing – A cost efficient way of solving unbalance problems*. URL: https://www.swerea.se/file/621/download?token=jAUjbOA4. accessed: 29.03.2019.

[2] B. Naik, P. Karunakar, M. Jayadev, and V. Marshal. "Role of Platelet rich fibrin in wound healing: A critical review". In: *Journal of Conservative Dentistry* Vol. 16 (2013), pp. 284–293.

[3] *Process for Platelet Rich Fibrin*. URL: https://medicalbone.nl/productinformatie/a-prf-advanced-platelet-rich-fibrin/. accessed: 29.03.2019.

[4] D. Dohan, J. Choukroun, A. Diss, A. Dohan, J. Mouhyi, and B. Gogly. "Platelet-rich fibrin (PRF): A second-generation platelet concentrate. Part I: Technological concepts and evolution". In: *Elsevier* Vol. 101 (2006), pp. 37–44.

[5] N. van de Wouw, N. van den Heuvel, and H. Nijmeijer. "Performance of an automatic ball balancer with dry friction". In: *International Journal of Bifurcation and Chaos* Vol. 15 (2004), pp. 65–82.

[6] Y. Ishida. "Recent development of the passive vibration control method". In: *Mechanical Systems and Signal Processing* Vol. 29 (2012), 2–18.

[7] M. van der Helm, S.J. van der Voort, R. Meijer, and J. Montagne. *Over het ontwerpproces van een add-on balancing ring voor een klinische centrifuge*.